Highly Stretchable and Sensitive Self-Powered Sensors Based on the N-Type Thermoelectric Effect of Polyurethane/$Na_x(Ni\text{-}ett)_n$/Graphene Oxide Composites

Kening Wan[1], Zilu Liu[2], Bob C. Schroeder[2], Guangming Chen[3], Giovanni Santagiuliana[1,4], Dimitrios G. Papageorgiou[1], Han Zhang[1], Emiliano Bilotti[1,4,]*

Dr. K. Wan, Dr. G. Santagiuliana, Dr. D. G. Papageorgiou, Dr. H. Zhang, Dr. E. Bilotti,

School of Engineering and Materials Science, Queen Mary University of London, Mile End Road, London, E1 4NS, UK
E-mail: e.bilotti@qmul.ac.uk
Dr. Z. Liu, Dr. B. C. Schroeder, Department of Chemistry, University College of London, 20 Gordon Street, London, WC1H 0AJ, UK
Prof. G. Chen, College of Materials Science and Engineering, Shenzhen University, Shenzhen 518055, P. R. China
Dr. G. Santagiuliana, Dr. E. Bilotti, Nanoforce Technology Ltd., Joseph Priestley Building, Queen Mary University of London, Mile End Road, London, E1 4NS, UK

Keywords: Stretchable device, sensors, self-powered sensors, organic thermoelectrics.

Abstract

The development of stretchable organic thermoelectric materials is prompted by fast evolving application fields like flexible electronic devices, soft robotics, health monitoring and internet-of-things. Stretchability in thermoelectric materials is usually obtained by using an insulating elastomer, either as a substrate or as a matrix in a blend or composite, which, unfortunately, leads to a compromise in thermoelectric performance. Herein, a potential solution is reported exploiting the addition of graphene oxide as a secondary (nano)filler in a polyurethane/poly nickel-ethenetetrathiolates film. Compared with traditional binary blends, our ternary composite shows an increased electrical conductivity (4 times), air-stability (~20 times after 3 months), and stretchability (38% increase in strain at break). With a gauge factor (GF) of ~ 58, this new composite film shows high sensitivity to tensile strain. Thanks to its Seebeck coefficient of ~ -40 $\mu V\ K^{-1}$, the composite film can generate a thermopower of ~0.25 pW when

subjected to a small temperature difference (30 °C), which could be exploited by self-powered strain sensors. Therefore, the ternary polyurethane/poly nickel-ethenetetrathiolates/graphene oxide composite film can work as a stretchable strain sensor, providing a strategy to reconcile the compromise between thermoelectric performance and stretchability.

1. Introduction

The thermoelectric (TE) effect, firstly discovered in the early 1800s, has been used extensively for temperature sensing, energy generation and cooling [1-3]. Over the last few years, organic thermoelectric (OTE) materials have attracted great interest as a replacement for traditional inorganic materials, owing to their lower toxicity, abundance of constitutive elements and ease in processing [4], with great potential in many fields, also in combination with solar cells [5, 6], supercapacitors [7] and gating transistors [8]. However, the relatively low thermoelectric properties of the OTE materials are still a major limiting factor for their wider applications. This is particularly true for n-type OTEs, which usually suffer also from poor environmental stability [9].

Different strategies to boost TE properties have been studied, including chemically [10, 11] or electrochemically [12] fine-tuning of the doping level, morphology optimisation [13, 14] or addition of nanofillers [15-19]. Among different nanofillers, carbon nanoparticles have been widely investigated [16-19], with two-dimensional graphene [20] and its derivatives attracting the most attention thanks to their excellent charge transport, mechanical properties and chemical stability [21]. Compared to the thermal conductivity of monolayer graphene (3000–

5000 $Wm^{-1}K^{-1}$ [22]), the thermal conductivity of graphene oxide (GO) is expected to be 2-3 orders of magnitudes lower ([23, 24]), leading to a positive effect on the dimensionless thermoelectric figure of merit, ZT ($ZT = \frac{\sigma\alpha^2}{\kappa}T$,). Moreover, GO can be synthesised relatively readily and in bulk by chemical oxidation, solvent-assisted exfoliation, or electrolytic oxidation of graphite [25].

Poly sodium nickel-ethenetetrathiolate ($Na_x(Ni\text{-}ett)_n$), an organometallic coordination polymer, is considered as one of the best performing n-type OTE [26-28][29]. To overcome its limited processability and toughness, our group has recently presented a highly stretchable n-type TE composite film based on $Na_x(Ni\text{-}ett)_n$ dispersed into a polyurethane matrix [30]. However, the presence of polyurethane as the continuous phase in the composite film limits the electrical conductivity and, consequently, the figure of merit of the composite film.

In this study, GO was introduced into the polyurethane/$Na_x(Ni\text{-}ett)_n$ film. We will show that the presence of GO could modify the film microstructure, which resulted in an increased electrical conductivity without affecting the Seebeck coefficient. Additionally, the GO sheets could protect the n-type $Na_x(Ni\text{-}ett)_n$ from degradation in air, enhancing the air-stability of the fabricated composite films and, consecutively, preserving their electrical conductivity. The mechanical properties and the sensitivity to strain of the films were also improved . Eventually, we will show that these films are able to convert energy from small temperature differences (~30 °C) thanks to their thermoelectric effect. The converted energy could be used by self-powered sensors to detect strain stimuli.

2. Experimental

2.1. Materials

Graphite flakes (99.8%, ~325 mesh, 43209) were purchased from Alfa Aesar. Sulfuric acid (>95%), sodium nitrate, potassium permanganate, hydrogen peroxide (35 wt.% in water), hydrochloric acid (37%), hydrogen peroxide (5%), 1,3,4,6-tetrathiapentalene-2,5-dione (TPD, 4.8 mmol), sodium methoxide (22.2 mmol), nickel (II) chloride (4.8 mmol) and dimethyl sulfoxide (DMSO, 99.9%) were purchased from Sigma Aldrich and used as received. Deionized water was used throughout all the experiments. $Na_x(Ni\text{-}ett)_n$ was synthesized following a reported procedure [27, 30]. Briefly, TPD was reacted with excess of sodium methoxide in refluxing methanol solution followed by adding nickel (II) chloride hexahydrate prepared from nickel (II) chloride, and then exposed to air for 30 minutes.

2.2. Preparation and purification of graphene oxide

A modified Hummers' method was used for synthesizing graphene oxide (GO) [31]. The mixture of graphite (5 g) and sodium nitrate (5 g) was dispersed in 230 mL sulphuric acid (>95%). Potassium permanganate (15 g) was added gradually while stirring in an ice-water bath, keeping the temperature of the mixture under 20 °C. After maintaining the mixture at 35 ±3 °C for 30 min, 460 mL deionized water were slowly added, and the temperature was increased to 98 °C. After 15 min, 25 mL of hydrogen peroxide diluted in 350 mL deionized water were added to the mixture. The final mixture was filtered and washed with 5% hydrochloric acid solution until sulphate could no longer be detected with $BaCl_2$. The resulting solid residue was suspended in water by ultrasonication for half an hour, followed by centrifugation at 4000 rpm for 10 min to remove aggregates. The graphite oxide was finally obtained by drying the supernatant under vacuum.

2.3. Preparation of $Na_x(Ni\text{-}ett)_n$/PU/GO composite films

5 wt.% $Na_x(Ni\text{-}ett)_n$ and 1 wt.% polyurethane (PU, Lycra® Invista) were dispersed in anhydrous DMSO (> 99.9 %, Sigma Aldrich), separately [30]. By mixing the two dispersions at a ratio of 1:5, the same solid content of $Na_x(Ni\text{-}ett)_n$ and PU was obtained in the mixture. 4 mg mL^{-1} graphite oxide was dispersed in DMSO by ultrasonication for 2 hours and added to the mixture in different amounts so that the content of GO in the final composite films was 0, 1, 2, 3 and 4 wt.%. The films were prepared by drop casting approximately 0.6 mL of mixture on pre-cleaned glass sides (pre-cut into 20 mm × 25 mm) and dried at 80 ℃ in a vacuum oven for 2 hours. According to the GO amount in the final composite films, the samples were named as NL, NL1GO, NL2GO, NL3GO and NL4GO, respectively. Self-standing films were fabricated by repeating the drop-casting procedure 6 times on a 40 mm × 25 mm glass slide until the weight of solid was approximately 0.1 g. Approximately 50 µm thickness was obtained after drying at 80 ℃ in a vacuum oven and peeling off.

2.5. Characterisations

The morphology of the samples was examined by field-emission scanning electron microscopy (FEI Inspect F) and transmission electron microscopy (TEM, JEOL JEM2010 200 kV). Fourier-transform infrared spectroscopy (FTIR) spectra of solution blends were recorded using a Bruker Tensor 27, with the DMSO signal eliminated from background in the range of 500–4000 cm^{-1}. X-ray diffraction (XRD) characterisations were performed using a diffractometer system XPERT-PRO employing the 1.54 Å Cu K-alpha wavelength.

The electrical conductivity was measured at room temperature and ambient atmosphere by a four-point probe setup (0.25 mm probe space) with an Agilent 6614 System DC power supply and a Keithley 6485 picoammeter connected to the external probes for monitoring the current through the samples. A high impedance Keithley 2000 Multimeter was used to record the voltage generated between the two internal probes. Films were cooled down to room temperature before electrical measurements (after about 10 min). Each film was measured five times at different points. The thickness of the samples was measured using a profilometer

(Bruker Dektak Vision 64) at ten different locations for each film and averaged for electrical conductivity calculation. The electrical conductivity was averaged out of five films for each GO content.

The Seebeck coefficient was measured by an MMR System (SB100 digital Seebeck controller and K20 digital temperature controller) at 300 K under nitrogen atmosphere for at least ten times on each film. The averaged result was calculated out of four films for each GO content.

Tensile strains on fabricated NLGO films (40 mm × 5 mm × 50 μm cut by a D882-02 standard die) and self-powered sensors were applied by a quasi-static tensile tester (Instron 5566) with a strain rate of 100% min^{-1}. The resistance variation during stretching was measured by an Agilent 34401A 6½ digital multimeter synchronised with the tensile tester. For the self-powered strain sensor demonstration, a heater pad (RS, 12 V dc, 7.5 W, item 245-556) was attached to one end of the film and set to 55 °C. A picoammeter (Keithley 6485) was used for measuring output currents while a multimeter (Keithley 2000) was used to measure synchronously the output voltage, by connecting to two ends of the external load.

3. Results and discussion

The exfoliated GO was analysed by SEM and TEM (**Figure S1&2** in the Supporting Information), as well as by XRD (**Figure S3**). An interlayer spacing of 0.8 nm was calculated using the Bragg's law. The natural graphite flakes before oxidation presented an interlayer spacing of 0.335 nm, meaning that, after the modified Hummers' method, a large number of oxygen-containing groups - like hydroxyl and epoxy groups on surfaces, carbonyl and carboxyl groups on the edges [32] -were introduced, which increased the interlayer spacing. A series of composite films based on PU, 50 wt.% a $Na_x(Ni\text{-}ett)_n$ and different amounts of GO ranging from 1 to 4 wt.% were prepared by solution blending and casting as described in the experimental section. The films were called NL, NL1GO, NL2GO, NL3GO and NL4GO according to the amount of GO they contained. It was found by XRD tests (**Figure S4**) that the (001) peak of GO appeared in the NLGO films, and its intensity increased with the amount of

GO. No changes could be observed for other peaks, meaning that the crystalline structure was not altered by the presence of GO.

The electrical conductivity (σ) of the films (**Figure 1a**) was tested by a four-point probe setup. The NL2GO films showed the highest conductivity, which is 5 times higher than that of the NL films. We believe that this effect was mainly due to the presence of GO, which modified the microstructural morphology of the films. Indeed, the SEM investigation (**Figure 1b** and **Figure S5**) on the films revealed smaller and better dispersed $Na_x(Ni\text{-}ett)_n$ agglomerates within the insulating polymer matrix, hence increasing the number of conductive pathways. The GO can enhance the dispersion of $Na_x(Ni\text{-}ett)_n$ particles and reduce agglomeration in the polymer matrix because of the large amount of functional groups on its edges and surface. These functional groups promote physical interaction between $Na_x(Ni\text{-}ett)_n$ and GO sheet, thus helping to disperse the particles and reduce their aggregation. Therefore, more robust conductive networks can be built by these well dispersed $Na_x(Ni\text{-}ett)_n$ compared with aggregated $Nax(Ni\text{-}ett)_n$ in the NL film. However, an excessive amount of electrically insulating GO (higher than 3wt%) creates an obstacle to the electrically conductive network, thus reducing the film's electrical conductivity. The Seebeck coefficient (S) of the films is presented in **Figure 1a**. Noticeably, the Seebeck coefficient was not affected by the addition of GO and remained around - 40 $\mu V\ K^{-1}$. Therefore, the corresponding power factor (PF, calculated as $PF=S^2\times\sigma$) of the NL2GO films is 7.35 $nW\ m^{-1}\ K^{-2}$, which is 4.5 times higher than that of the NL films without any GO (1.64 $nW\ m^{-1}\ K^{-2}$). The decoupling of σ and S, namely the invariance of the Seebeck coefficient combined with an increase in electrical conductivity, is in agreement with the assumption that a change in composite morphology is the dominant mechanism in our case.

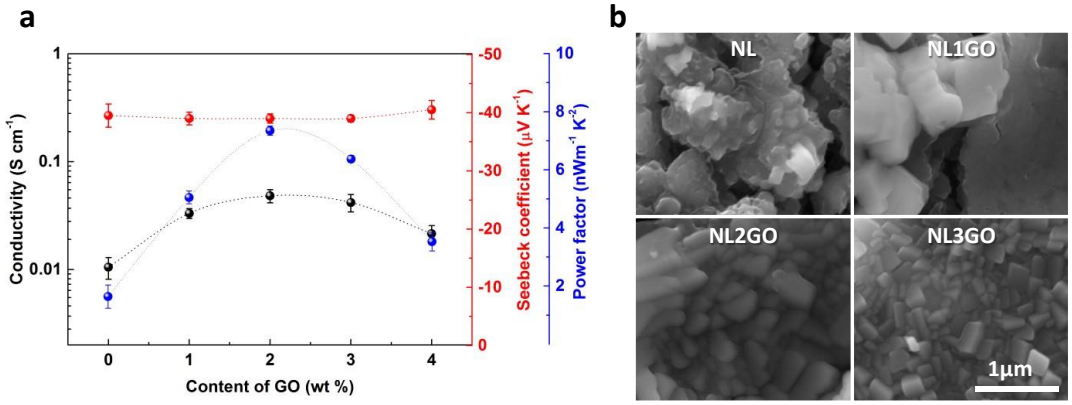

Figure 1 *TE properties and morphologies of the NLGO composite films. (a) Electrical conductivity, Seebeck coefficient and PF as a function of GO content. (b) SEM images of the NLGO composite films, showing a clear morphological change from agglomerated clusters to a more well-dispersed and connected network of* $Na_x(Ni\text{-}ett)_n$ *particles.*

Apart from improving the TE performance, the two-dimensional nature of GO can also modify the barrier and transport properties of the composites. It was observed that after 1 hour from casting, the electrical conductivity of the NLGO films increased (**Figure 2a**). This is likely due to a morphology effect during the formation of the films: it is reasonable to assume that the presence of GO in our composites slowed down the solvent evaporation and solvent evaporation time during film casting is a known parameter affecting film morphology [33] [34]. Moreover, although $Na_x(Ni\text{-}ett)_n$ is reported as a relatively air-stable n-type TE material [35], the NL films showed a degradation in electrical conductivity, which dropped from 0.01 S cm^{-1} to less than 3×10^{-4} S cm^{-1} after being exposed to air at room temperature for 3 months (**Figure 2a**). This could be due to a degradation of the composite film as a result of gas diffusion within the films. Contrarily, NLGO films showed a lower decrease in electrical conductivity over time. The electrical conductivity of the NL1GO films only reduced to 0.0025 S cm^{-1} after 3 months exposure to air at room temperature, which is 8 times higher than that of the NL films. Higher GO contents resulted in even greater effects. The improved air-stability of the NLGO films could be caused by the gas barrier effect of GO. After 3 months, the Seebeck coefficient of the

NL films did not change, whereas the electrical conductivity of the NL4GO films, and thus the *PF*, is 15 times higher than that of the NL films.

A more systematic study on the effect of degradation time and temperature was carried out on the NL2GO films (**Figure 2b-d)**. The NL2GO films can maintain their electrical conductivity (0.025 S cm^{-1}) constant over 60 days, while the NL films reduced their conductivity from 0.015 to 0.001 S cm^{-1}. This trend was also verified under accelerated degradation conditions at high temperatures. After 2 months at 80 °C or 120 °C, the electrical conductivity of the NL2GO was one or two orders of magnitude higher than that of the NL films, respectively.

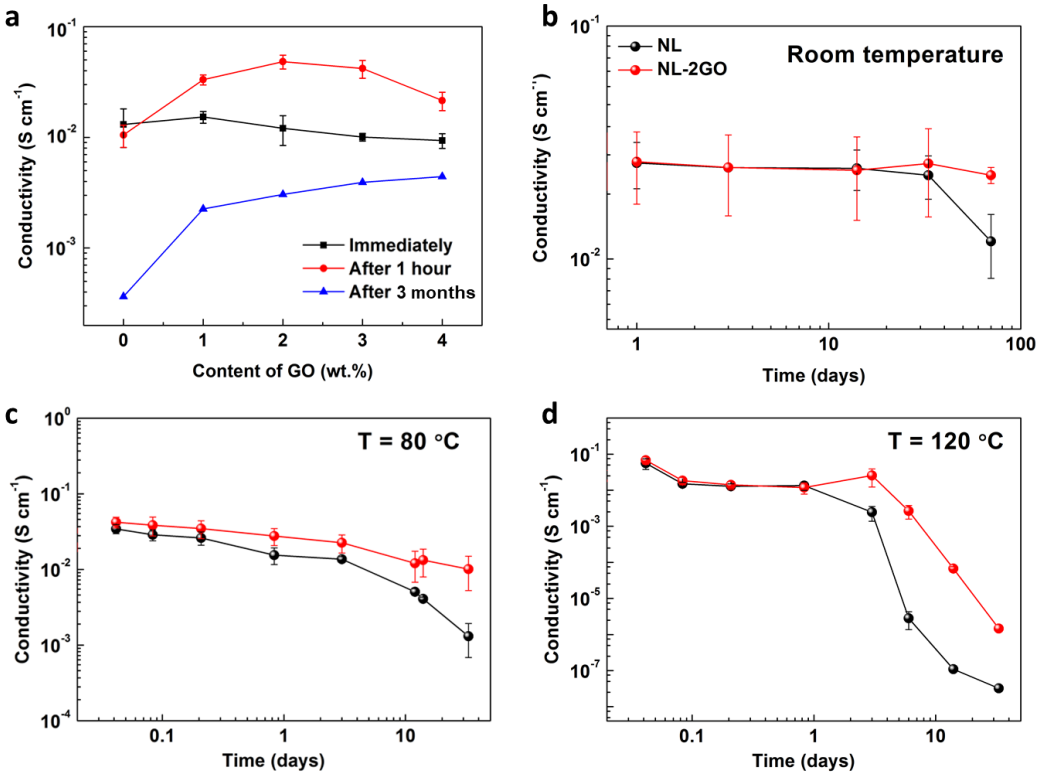

Figure 2 *The effect of GO content on the electrical conductivity of the films over time. (a) Electrical conductivity of the NL films containing various amounts of GO after exposure to air for different durations. Change of electrical conductivity of the NL (black) and NL2GO films (red) after exposure to air (relative humidity ~ 70%) at (b) room temperature, (c) 80 °C and (d) 120 °C over time.*

The stress-strain curves in **Figure 3a** represent the mechanical response of the NL and NL2GO films. The strain-at-break and elastic modulus increased from 400 ± 17 % and 24 ± 2 MPa for the NL films to 550 ± 24% and 78 ± 8 MPa for the NL2GO films, respectively. The increase in Young's modulus with the addition of GO is expected following the typical reinforcing effect imparted by rigid fillers/particles to polymer composites [36] [37]. However, this is usually followed by an embrittlement of the composite. In our case, the simultaneous increase in Young's modulus, strength, strain-at-break and toughness can be explained by the change in composite morphology previously formulated. The presence of GO prevented the $Na_x(Ni\text{-}ett)_n$ particles from agglomerating within the polymer matrix and allowed a better dispersion.

During the tensile tests, the electrical resistance was also synchronously measured to evaluate the strain sensitivity of the composite films (**Figure 3b**). The resistance increased monotonically and approximately linearly with the tensile deformation. The sensitivity of a strain sensor is normally evaluated by the gauge factor (*GF*), defined as $GF = (\Delta R/R_0)/\varepsilon$, where $\Delta R = R - R_0$ is the difference between the electrical resistance at a given extension (R) and the initial resistance (R_0), and ε is the strain. The NL2GO films showed a nearly 6 times greater strain sensitivity compared with NL films (GF ~58 vs. ~9.8). Notably, the same gauge factor was maintained even for strains as high as 300%. This result is important as it overcomes the typical compromise between high *GF* values (>50) and high strain ranges (>300%) [38-56]. The NL2GO films were further subjected to cyclic tensile strain tests (**Figure 3c**). In the strain range of 5, 10, 30, 50, 80 100 and 150%, clear and reversible sensing strain signals were obtained.

Because of their thermoelectric properties, the NL2GO films could generate a voltage that could be used to power strain sensors. To demonstrate this concept, a constant temperature difference (ΔT ~ 30 °C) was applied to the films by attaching a heat pad (~ 55 °C) to one end of the films within one clamp of the tensile tester (**Figure 3d**). When the samples were connected to a resistor (R_L ~30 kΩ), a thermoelectric power ($P_{(R_L \sim 30\ k\Omega)} = I_{(R_L \sim 30\ k\Omega)} \times U_{(R_L \sim 30\ k\Omega)}$) ~0.25 pW was generated, and both the current and voltage output were recorded. Under various

cyclic strains (5, 10, 30, and 50%), both current and voltage changed simultaneously (**Figure 3e**). This is due to a decrease in the thermal current generated ($I(\varepsilon) = \frac{S \times \Delta T}{Rs(\varepsilon)+R_L}$) as the resistance of the sample (R_s) increases with the strain (ε). Consequently, also the voltage (V) measured across the load resistor decreased with the strain ($V(\varepsilon) = I(\varepsilon)R_L$). Therefore, either the current output or the voltage output can be used to sense the deformation. For a self-powered sensor integrated with a signal recording/transmitting system, based on the energy provided by the thermoelectric effect of our films, higher power and voltage outputs would be necessary. This could be achieved either by increasing the temperature gradient or by connecting n-type legs, with suitable p-type counterparts, in series [30]. For applications such as wearable sensors, the temperature gradient is normally smaller than 30 °C. Therefore, a series of p–n junctions is more reasonable. This could be achieved by connecting the n-type NL2GO films to stretchable p-type OTEs such as those based on PU/PEDOT:PSS films [56]. We estimate that three thousand couples based on n-type NL2GO films (half the number by using NL film) and p-type PU/PEDOT:PSS films [56] under a gradient ΔT ~30 °C would be able to generate a power output of 10 μW (see **Note S1**), able to integrate a strain sensor in a self-powered mode. Based on the size estimation ($57\ cm^3$) the device will be small enough to be transported and worn.

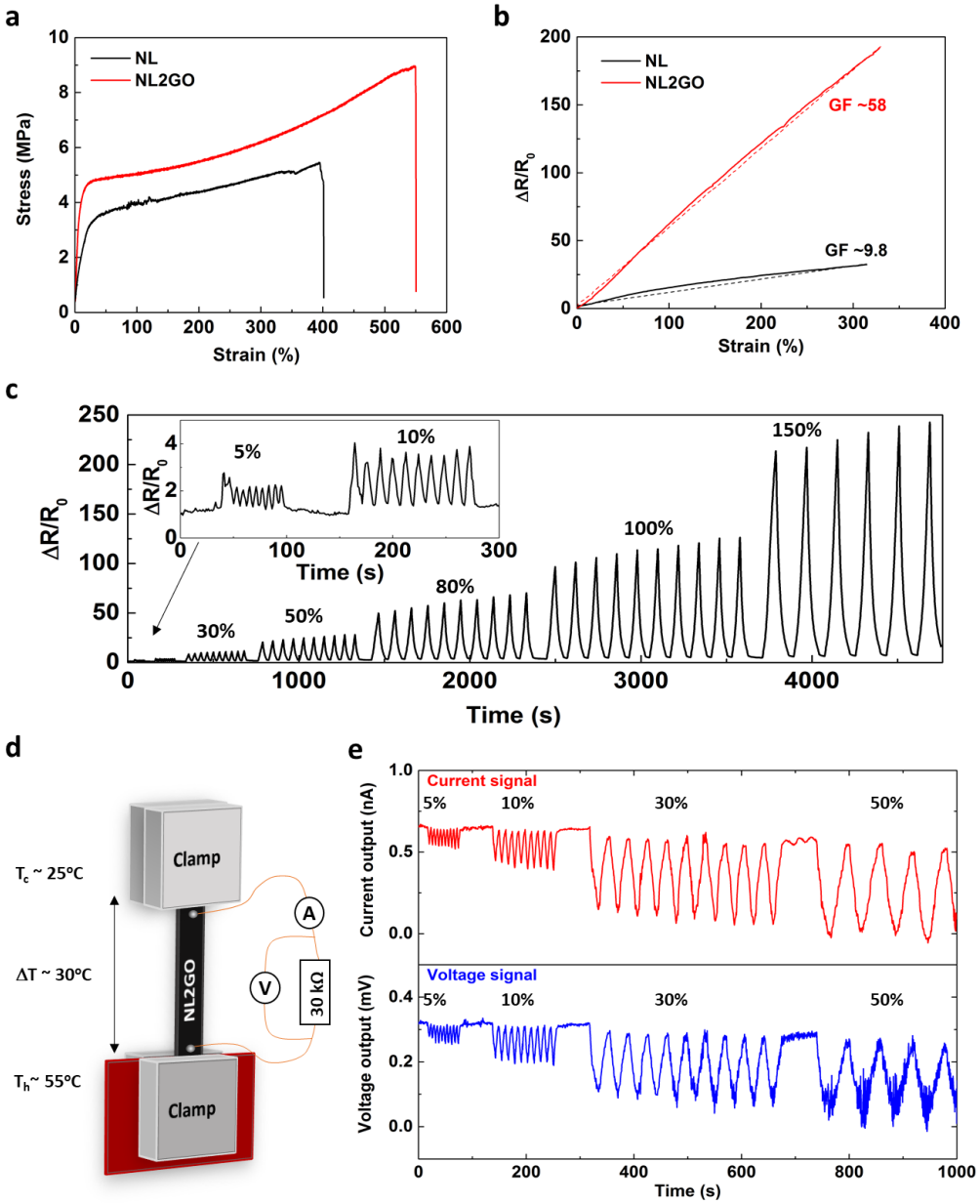

Figure 3 *Mechanical and strain sensing investigations of the NL2GO films. (a) Typical stress-strain curves of the NL2GO and NL films, and (b) their resistance variation ($\Delta R/R_0$) and corresponding gauge factor as a function of the applied strain. (c) Resistance variation of the NL2GO films under cyclic tensile strains. (d) Illustration of the set-up and electrical circuit used to measure the voltage and current outputs generated by the NL2GO films. (e) Corresponding real-time signals when a NL2GO film was subjected to cyclic strains.*

4. Conclusions

The effect of GO sheets on the thermoelectric properties of n-type PU/$Na_x(Ni\text{-}ett)_n$ composites films was studied. GO was demonstrated to modify the morphology of the composites enhancing the dispersion of $Na_x(Ni\text{-}ett)_n$ crystal particles with reduced agglomerates within the polymer matrix. Consequently, a 4 folds increase in electrical conductivity was obtained together with an increase in strain at break of 38% and an improvement of the Young's modulus of 200% when the films contained a GO concentration of 2 wt.%. Additionally, the good barrier properties of GO improved the environmental stability of $Na_x(Ni\text{-}ett)_n$, preserving its electrical conductivity for a prolonged period. After exposure to air, at ambient conditions for 3 months, the electrical conductivity of the NL2GO films were two orders of magnitudes higher than that of pristine NL films.

PU composites films containing both $Na_x(Ni\text{-}ett)_n$ and 2 wt.% GO were also tested for their strain sensing properties. An unusually high sensitivity to strain (GF ~58) over a strain range as high as 550% was reported. Because of their thermoelectric properties (Seebeck coefficient of ~ -40 $\mu V\ K^{-1}$), these films can generate energy that could be used to integrate a strain sensor in a self-powered mode.

Supporting Information

Supporting Information is available from online or from the author.

Acknowledgements

Kening Wan and Zilu Liu are grateful to the China Scholarship Council for the scholarship supporting. B.C.S. acknowledges the UK Research and Innovation for Future Leaders

Fellowship no. MR/S031952/1. G.C acknowledges the financial supports by Royal Society International Exchanges Grant (IEC/NSFC/191473) and National Natural Science Foundation of China (52011530178).

References

[1] F.J. DiSalvo, Thermoelectric Cooling and Power Generation, Science 285(5428) (1999) 703-706.
[2] S. Twaha, J. Zhu, Y. Yan, B. Li, A comprehensive review of thermoelectric technology: Materials, applications, modelling and performance improvement, Renewable and Sustainable Energy Reviews 65 (2016) 698-726.
[3] L. Zhang, X. Han, M. Du, Y. Shi, K. Zhang, Compliant three-dimensional thermoelectric generator filled with porous PDMS for power generation and solid-state cooling, Composites Communications 26 (2021) 100793.
[4] P.J. Taroni, I. Hoces, N. Stingelin, M. Heeney, E. Bilotti, Thermoelectric Materials: A Brief Historical Survey from Metal Junctions and Inorganic Semiconductors to Organic Polymers, Israel Journal of Chemistry 54(5-6) (2014) 534-552.
[5] D. Kraemer, L. Hu, A. Muto, X. Chen, G. Chen, M. Chiesa, Photovoltaic-thermoelectric hybrid systems: A general optimization methodology, Applied Physics Letters 92(24) (2008) 243503.
[6] N. Wang, L. Han, H. He, N.-H. Park, K. Koumoto, A novel high-performance photovoltaic–thermoelectric hybrid device, Energy & Environmental Science 4(9) (2011) 3676-3679.
[7] D. Zhao, H. Wang, Z.U. Khan, J.C. Chen, R. Gabrielsson, M.P. Jonsson, M. Berggren, X. Crispin, Ionic thermoelectric supercapacitors, Energy Environ. Sci. 9(4) (2016) 1450-1457.
[8] D. Zhao, S. Fabiano, M. Berggren, X. Crispin, Ionic thermoelectric gating organic transistors, Nat Commun 8 (2017) 14214.
[9] Y. Sun, C.-A. Di, W. Xu, D. Zhu, Advances in n-Type Organic Thermoelectric Materials and Devices, Adv. Electron. Mater. 5(11) (2019) 1800825.
[10] Y. Jia, Q. Jiang, B. Wang, Z. Ma, D. Zhao, N. Zheng, J. Zhou, P. Liu, D. Hu, Y. Ma, Utilizing perylene diimmide as dopant to improve thermoelectric performance of PEDOT:PSS films, Composites Communications 27 (2021) 100844.
[11] B.P. Tripathi, V.K. Shahi, Organic–inorganic nanocomposite polymer electrolyte membranes for fuel cell applications, Prog. Polym. Sci. 36(7) (2011) 945-979.
[12] W.B. Chang, H. Fang, J. Liu, C.M. Evans, B. Russ, B.C. Popere, S.N. Patel, M.L. Chabinyc, R.A. Segalman, Electrochemical Effects in Thermoelectric Polymers, ACS Macro Letters 5(4) (2016) 455-459.

[13] L.D. Hicks, M.S. Dresselhaus, Thermoelectric figure of merit of a one-dimensional conductor, Physical Review B 47(24) (1993) 16631-16634.
[14] Y. Wang, J. Zhou, R. Yang, Thermoelectric Properties of Molecular Nanowires, The Journal of Physical Chemistry C 115(49) (2011) 24418-24428.
[15] B. Zhang, J. Sun, H. Katz, F. Fang, R. Opila, Promising thermoelectric properties of commercial PEDOT: PSS materials and their Bi2Te3 powder composites, ACS applied materials & interfaces 2(11) (2010) 3170-3178.
[16] D. Kim, Y. Kim, K. Choi, J.C. Grunlan, C. Yu, Improved thermoelectric behavior of nanotube-filled polymer composites with poly (3, 4-ethylenedioxythiophene) poly (styrenesulfonate), ACS nano 4(1) (2009) 513-523.
[17] Q. Yao, L. Chen, W. Zhang, S. Liufu, X. Chen, Enhanced Thermoelectric Performance of Single-Walled Carbon Nanotubes/Polyaniline Hybrid Nanocomposites, ACS Nano 4(4) (2010) 2445-2451.
[18] C. Meng, C. Liu, S. Fan, A Promising Approach to Enhanced Thermoelectric Properties Using Carbon Nanotube Networks, Adv. Mater. 22(4) (2010) 535-539.
[19] C. Yu, K. Choi, L. Yin, J.C. Grunlan, Light-weight flexible carbon nanotube based organic composites with large thermoelectric power factors, ACS nano 5(10) (2011) 7885-7892.
[20] D. Zhang, K. Zhang, Y. Wang, Y. Wang, Y. Yang, Thermoelectric effect induced electricity in stretchable graphene-polymer nanocomposites for ultrasensitive self-powered strain sensor system, Nano Energy 56 (2019) 25-32.
[21] A.K. Geim, K.S. Novoselov, The rise of graphene, Nanoscience and technology: a collection of reviews from nature journals, World Scientific2010, pp. 11-19.
[22] Y. Wang, Y. Zhang, Superior thermal conductivity of carbon nanoscroll based thermal interface materials, 2015 IEEE 65th Electronic Components and Technology Conference (ECTC), 2015, pp. 1234-1239.
[23] J. Chen, L. Li, Thermal Conductivity of Graphene Oxide: A Molecular Dynamics Study, JETP Letters 112(2) (2020) 117-121.
[24] A.A. Balandin, Thermal properties of graphene and nanostructured carbon materials, Nat Mater 10(8) (2011) 569-81.
[25] L. Li, D. Zhang, J. Deng, Q. Kang, Z. Liu, J. Fang, Y. Gou, Review—Progress of Research on the Preparation of Graphene Oxide via Electrochemical Approaches, J. Electrochem. Soc. 167(15) (2020) 155519.
[26] Y. Sun, P. Sheng, C. Di, F. Jiao, W. Xu, D. Qiu, D. Zhu, Organic Thermoelectric Materials and Devices Based on p-and n-Type Poly (metal 1, 1, 2, 2-ethenetetrathiolate) s, Adv. Mater. 24(7) (2012) 932-937.
[27] A.K. Menon, E. Uzunlar, R.M. Wolfe, J.R. Reynolds, S.R. Marder, S.K. Yee, Metallo-organic n-type thermoelectrics: Emphasizing advances in nickel-ethenetetrathiolates, Journal of Applied Polymer Science 134(3) (2017).

[28] Y. Sun, L. Qiu, L. Tang, H. Geng, H. Wang, F. Zhang, D. Huang, W. Xu, P. Yue, Y.-s. Guan, F. Jiao, Y. Sun, D. Tang, C.-a. Di, Y. Yi, D. Zhu, Flexible n-Type High-Performance Thermoelectric Thin Films of Poly(nickel-ethylenetetrathiolate) Prepared by an Electrochemical Method, Adv. Mater. 28(17) (2016) 3351-3358.
[29] Z. Liu, T. Liu, C.N. Savory, J.P. Jurado, J.S. Reparaz, J. Li, L. Pan, C.F.J. Faul, I.P. Parkin, G. Sankar, S. Matsuishi, M. Campoy-Quiles, D.O. Scanlon, M.A. Zwijnenburg, O. Fenwick, B.C. Schroeder, Controlling the Thermoelectric Properties of Organometallic Coordination Polymers via Ligand Design, Adv. Funct. Mater. 30(32) (2020) 2003106.
[30] K. Wan, P.T. Junior, Z. Liu, Y. Liu, G. Santagiuliana, Y. Tu, H. Zhang, O. Fenwick, S. Krause, M. Baxendale, Flexible Self-powered Sensors by Using Organic Thermoelectric Effect.
[31] K. Wan, S. Liu, C. Zhang, L. Li, Z. Zhao, T. Liu, Y. Xie, Supramolecular Assembly of 1D Pristine Carbon Nanotubes and 2D Graphene Oxides into Macroscopic All-Carbon Hybrid Sponges for High-Energy-Density Supercapacitors, ChemNanoMat 3(6) (2017) 447-453.
[32] D.R. Dreyer, S. Park, C.W. Bielawski, R.S. Ruoff, The chemistry of graphene oxide, Chemical Society Reviews 39(1) (2010) 228-240.
[33] C. Schaefer, J.J. Michels, P. van der Schoot, Structuring of Thin-Film Polymer Mixtures upon Solvent Evaporation, Macromolecules 49(18) (2016) 6858-6870.
[34] A.A. Virkar, S. Mannsfeld, Z. Bao, N. Stingelin, Organic Semiconductor Growth and Morphology Considerations for Organic Thin-Film Transistors, Adv. Mater. 22(34) (2010) 3857-3875.
[35] R.M.W. Wolfe, A.K. Menon, T.R. Fletcher, S.R. Marder, J.R. Reynolds, S.K. Yee, Simultaneous Enhancement in Electrical Conductivity and Thermopower of n-Type NiETT/PVDF Composite Films by Annealing, Adv. Funct. Mater. 28(37) (2018) 1803275.
[36] Y. Gao, O.T. Picot, E. Bilotti, T. Peijs, Influence of filler size on the properties of poly(lactic acid) (PLA)/graphene nanoplatelet (GNP) nanocomposites, European Polymer Journal 86 (2017) 117-131.
[37] E. Bilotti, H. Deng, R. Zhang, D. Lu, W. Bras, H.R. Fischer, T. Peijs, Synergistic Reinforcement of Highly Oriented Poly(propylene) Tapes by Sepiolite Nanoclay, Macromolecular Materials and Engineering 295(1) (2010) 37-47.
[38] M. Amjadi, Y.J. Yoon, I. Park, Ultra-stretchable and skin-mountable strain sensors using carbon nanotubes–Ecoflex nanocomposites, Nanotechnology 26(37) (2015) 375501.
[39] S. Gong, D.T.H. Lai, B. Su, K.J. Si, Z. Ma, L.W. Yap, P. Guo, W. Cheng, Highly Stretchy Black Gold E-Skin Nanopatches as Highly Sensitive Wearable Biomedical Sensors, Advanced Electronic Materials 1(4) (2015) 1400063.
[40] C.S. Boland, U. Khan, C. Backes, A. O'Neill, J. McCauley, S. Duane, R. Shanker, Y. Liu, I. Jurewicz, A.B. Dalton, J.N. Coleman, Sensitive, High-Strain, High-Rate Bodily Motion Sensors Based on Graphene–Rubber Composites, ACS Nano 8(9) (2014) 8819-8830.
[41] S. Gong, D.T.H. Lai, Y. Wang, L.W. Yap, K.J. Si, Q. Shi, N.N. Jason, T. Sridhar, H. Uddin, W. Cheng, Tattoolike Polyaniline Microparticle-Doped Gold Nanowire Patches as Highly Durable Wearable Sensors, ACS Applied Materials & Interfaces 7(35) (2015) 19700-19708.

[42] X. Xiao, L. Yuan, J. Zhong, T. Ding, Y. Liu, Z. Cai, Y. Rong, H. Han, J. Zhou, Z.L. Wang, High-Strain Sensors Based on ZnO Nanowire/Polystyrene Hybridized Flexible Films, Adv. Mater. 23(45) (2011) 5440-5444.
[43] D. Kang, P.V. Pikhitsa, Y.W. Choi, C. Lee, S.S. Shin, L. Piao, B. Park, K.-Y. Suh, T.-i. Kim, M. Choi, Ultrasensitive mechanical crack-based sensor inspired by the spider sensory system, Nature 516(7530) (2014) 222-226.
[44] N. Lu, C. Lu, S. Yang, J. Rogers, Highly Sensitive Skin-Mountable Strain Gauges Based Entirely on Elastomers, Adv. Funct. Mater. 22(19) (2012) 4044-4050.
[45] E. Roh, B.-U. Hwang, D. Kim, B.-Y. Kim, N.-E. Lee, Stretchable, Transparent, Ultrasensitive, and Patchable Strain Sensor for Human–Machine Interfaces Comprising a Nanohybrid of Carbon Nanotubes and Conductive Elastomers, ACS Nano 9(6) (2015) 6252-6261.
[46] Y.R. Jeong, H. Park, S.W. Jin, S.Y. Hong, S.-S. Lee, J.S. Ha, Highly Stretchable and Sensitive Strain Sensors Using Fragmentized Graphene Foam, Adv. Funct. Mater. 25(27) (2015) 4228-4236.
[47] C. Mattmann, F. Clemens, G. Tröster, Sensor for measuring strain in textile, Sensors-Basel 8(6) (2008) 3719-3732.
[48] J.T. Muth, D.M. Vogt, R.L. Truby, Y. Mengüç, D.B. Kolesky, R.J. Wood, J.A. Lewis, Embedded 3D Printing of Strain Sensors within Highly Stretchable Elastomers, Adv. Mater. 26(36) (2014) 6307-6312.
[49] J.-H. Kong, N.-S. Jang, S.-H. Kim, J.-M. Kim, Simple and rapid micropatterning of conductive carbon composites and its application to elastic strain sensors, Carbon 77 (2014) 199-207.
[50] B.-U. Hwang, J.-H. Lee, T.Q. Trung, E. Roh, D.-I. Kim, S.-W. Kim, N.-E. Lee, Transparent Stretchable Self-Powered Patchable Sensor Platform with Ultrasensitive Recognition of Human Activities, ACS Nano 9(9) (2015) 8801-8810.
[51] M. Amjadi, A. Pichitpajongkit, S. Lee, S. Ryu, I. Park, Highly Stretchable and Sensitive Strain Sensor Based on Silver Nanowire–Elastomer Nanocomposite, ACS Nano 8(5) (2014) 5154-5163.
[52] M. Amjadi, K.-U. Kyung, I. Park, M. Sitti, Stretchable, Skin-Mountable, and Wearable Strain Sensors and Their Potential Applications: A Review, Adv. Funct. Mater. 26(11) (2016) 1678-1698.
[53] S. Han, C. Liu, X. Lin, J. Zheng, J. Wu, C. Liu, Dual Conductive Network Hydrogel for a Highly Conductive, Self-Healing, Anti-Freezing, and Non-Drying Strain Sensor, ACS Applied Polymer Materials 2(2) (2020) 996-1005.
[54] J. Wu, Z. Wu, X. Lu, S. Han, B.-R. Yang, X. Gui, K. Tao, J. Miao, C. Liu, Ultrastretchable and Stable Strain Sensors Based on Antifreezing and Self-Healing Ionic Organohydrogels for Human Motion Monitoring, ACS Applied Materials & Interfaces 11(9) (2019) 9405-9414.
[55] Z. Duan, Y. Jiang, S. Wang, Z. Yuan, Q. Zhao, G. Xie, X. Du, H. Tai, Inspiration from Daily Goods: A Low-Cost, Facilely Fabricated, and Environment-Friendly Strain Sensor Based on Common Carbon Ink and Elastic Core-Spun Yarn, ACS Sustainable Chemistry & Engineering 7(20) (2019) 17474-17481.

[56] P.J. Taroni, G. Santagiuliana, K. Wan, P. Calado, M. Qiu, H. Zhang, N.M. Pugno, M. Palma, N. Stingelin-Stutzman, M. Heeney, O. Fenwick, M. Baxendale, E. Bilotti, Toward Stretchable Self-Powered Sensors Based on the Thermoelectric Response of PEDOT:PSS/Polyurethane Blends, Adv. Funct. Mater. 28(15) (2018) 1704285.